JOURNAL OF APPLIED ELECTROCHEMISTRY 13 (1983) 751–764

Studies concerning the growth of cadmium dendrites. I. Morphology in alkaline media

R. BARNARD, G. S. EDWARDS, J. HOLLOWAY, F. L. TYE

Berec Group Limited, Group Technical Centre, St. Ann's Road, London N15 3TJ UK

Received 31 January 1983

The morphology of cadmium dendrites formed during potentiostatic electrodeposition onto nickel and cadmium substrates from cadmate solutions in alkaline supporting electrolyte has been investigated. The morphology is potential dependent for deposition under convective diffusion conditions to a nickel substrate. For 1.05×10^{-4} mol dm^{-3} $Cd(OH)_4^{2-}$/30% KOH solutions, 2D- fern dendrites are observed at an overpotential of -150 mV, needle dendrites at -200 mV, and large 'filled-in' fern dendrites at -300 mV. Similar results were found at the higher concentration, 2.4×10^{-4} mol dm^{-3} $Cd(OH)_4^{2-}$/50% KOH, but the time taken to grow an equivalent morphology and length were reduced in proportion.

Crystalline aggregate dendrites were observed on a cadmium substrate in 1.05×10^{-4} mol dm^{-3} $Cd(OH)_4^{2-}$/30% KOH, becoming more crystalline and well defined with increase in overpotential.

A significant induction time of the order 8 h was observed for all deposition onto stationary nickel and cadmium wires.

Under the well-defined diffusion conditions at a rotating nickel disc electrode only one morphology, namely small ferns, was observed over a wide range of overpotentials. The current–time behaviour is presented, and the current is shown to have a $(\text{time})^2$ dependence, indicative of progressive nucleation of dendrites. The induction time, indicated approximately by the current minima, had decreased significantly.

1. Introduction

Growth of cadmium deposits between the electrodes of the sealed nickel–cadmium cell system leading to a short circuit is commonly invoked as the cause of poor charge retention or cell failure [1–4]. Such deposits are usually termed 'dendritic' in type, although such a morphology may not be displayed, nor is it essential to cause abnormal behaviour. Direct visual evidence for metallic cadmium causing the electronic shunt paths is difficult to obtain and is usually inferred indirectly from electrical measurements or from the presence of $Cd(OH)_2$ within the separator [3].

There are several qualitative studies concerning dendrite growth [5–6] but quantitative data is sparse. Wranglen [7] has investigated growth of cadmium and silver dendrites from acetate and halide electrolytes, however, detailed observations concerning cadmium dendrites in alkaline solution have not been reported.

The general theory of dendrite growth appears to be fairly well developed and has been applied to favourable systems. Barton and Bockris [8] made the first attempt to relate the various dendrite growth parameters for silver using a fused salt system. Diggle *et al.* [9] then extended the study to growth of zinc dendrites from alkaline media. Both these studies drew attention to the importance of observing dendrite length with time as a function of overpotential and concentration and also the morphology of the deposit. Subsequent theories [10, 11] have relied heavily on the basic concepts laid down by Barton and Bockris [8] whilst extending the theory to cover a wider range of experimental conditions.

Dendrite growth is commonly regarded as an extension of the process of amplification of surface roughness [12]; the initial deposit following the surface macro-profile. A dendrite can be regarded as the skeleton of a mono-crystal consisting of a stalk and branches resembling a tree or fern. The dendrite tip-angle and the angles between the branches usually take up well defined values in

0021-891X/83 $03.00 + .12

accordance with the space lattice of the depositing metal. It is this feature of well-developed crystallinity coupled with the tendency to grow outwards from the substrate at high rates which distinguish dendrites from other types of deposit.

Several conditions appear to be required before dendrite growth takes place and these can be summarised as follows:

(a) A minimum overpotential η_c, is required before dendrites appear.

(b) There is an induction period prior to dendrite growth.

(c) There is an optimum tip radius for maximum rate of growth.

(d) The total current increases with time at constant potential once dendrites have been initiated.

(e) The yield of dendrites increases with overpotential above η_c.

(f) The length of dendrites increases exponentially with time whilst the dendrites are growing within the Nernst diffusion layer (appropriate to the planar substrate).

(g) Dendrite growth appears to be nearly linear with time for dendrite lengths exceeding the Nernst diffusion layer thickness.

The object of this study was to determine the range of experimental parameters which govern the occurrence and morphology of cadmium dendrites on nickel and cadmium substrates in alkaline medium. This system is, however, difficult to study because of the low solubility of cadmate [1.05×10^{-4} mol dm^{-3} at 25° C in 30% (7 mol dm^{-3}) KOH] necessitating long deposition times to grow relatively small dendrites. Simultaneous evolution of hydrogen is also an added complication. For this reason a parallel investigation was also undertaken concerning the deposition of cadmium onto a cadmium substrate in an acidic medium ($CdSO_4$ in 0.5 mol dm^{-3} H_2SO_4). In this way a range of depositing cation concentration from 10^{-1} to 10^{-4} mol dm^{-3} could be examined more readily and the complications from hydrogen evolution also largely avoided.

The first part of this investigation will be devoted largely to a scanning electron microscopy examination of various dendrites grown from cadmate in 30% or 50% KOH. In the second part dendrites grown from $CdSO_4/H_2SO_4$ will similarly be compared. The third part will deal with measurements taken from the SEM micrographs combined with the electrochemical data to gain further understanding of the parameters controlling the growth of cadmium dendrites.

2. Experimental procedure

2.1. *Apparatus and procedure*

Electrodeposition of cadmium onto nickel or cadmium substrates was performed both galvanostatically and potentiostatically (Chemical Electronics Potentiostat IC 20-0.5A and Witton Electronics type T7). The electrochemical cell was of a conventional design employing a cadmium wire counter electrode and usually a $Cd/Cd(OH)_4^{2-}$/ 7 mol dm^{-3} KOH reference electrode. Cadmium electrode potentials were additionally checked against an Hg/HgO/7 mol dm^{-3} KOH reference electrode. The Cd-counter and reference electrode system was preferred because it prevented possible contamination of the working solution by unwanted metal ions.

In some experiments a nickel rotating disc electrode (cross-sectional area, 0.196 cm^2) was employed at a fixed rotation speed (160.5 rad s^{-1}). Electrode rotation was controlled by means of a Chemical Electronics motor/control unit type R.P.1.

Electrolytes were thoroughly purged with argon before use (minimum $1\frac{1}{2}$ h) to remove dissolved oxygen. Electrodeposition experiments were made at overpotentials η up to $-$ 500 mV in potentiostatic experiments or over a range of current densities from 0.1–10 mA cm^{-2} in galvanostatic experiments. Electrodeposition was carried out over periods from 1–168 h.

In preliminary experiments the nickel rotating disc electrodes (RDE) surface was cathodized in 7 mol dm^{-3} KOH for 16 h at potentials in the hydrogen evolution region ($-$ 1400 mV wrt Hg/HgO/7 mol dm^{-3} KOH) in an attempt to remove any surface hydroxide/oxide films before immediate transfer to the working solution (7 mol dm^{-3} KOH containing 1.05×10^{-4} mol dm^{-3} $Cd(OH)_4^{2-}$). It was found that electrode cathodization influenced the shape of the initial current–time curves but had minor influence on the overall morphology of the deposit. Consequently for long-term deposition experiments the pretreatment procedure was omitted.

In potentiostatic experiments the current–time curves at constant potential were following continuously by means of a y–t recorder (Smiths 'Servoscribe') connected in parallel with a standard resistor in the counter-electrode circuit. In galvanostatic experiments, only the total charge flowing was monitored, the prime objective being observation of the final morphology of the deposit.

2.2. *Electrodes*

Samples of nickel and cadmium wire (1 mm diameter, purity 99.999% supplied by Koch-Light) were moulded in epoxy-resin to give a cylindrical electrode ~ 1 cm diameter and length ~ 5 cm. One end of the wire was sectioned, abraded and polished to give an optically flat surface using a progression of diamond pastes (14 μm down to 1/4 μm with Dialap lubricant). Some wires were used in an abraded (P600 SiC grade) only condition. Rotating disc electrodes were fabricated from 5 mm diameter rods to the respective metals (99.999% purity) and sheathed in PTFE mounts provided with suitable mechanical coupling to the rotating disc control unit.

After the deposition process was completed, the cadmium electrodes were washed thoroughly with argon saturated water and ethanol and dried under vacuum.

2.3. *Electrolytes*

Both 30 wt % (7 mol dm^{-3}) and 50 wt % (12.4 mol dm^{-3}) KOH were used as supporting electrolyte containing respectively 1.05 and 2.4×10^{-4} mol dm^{-3} of $Cd(OH)_4^{2-}$. This solution was prepared by adding $Cd(OH)_2$ to the alkali, shaking vigorously, and then allowing the solution to stand for several days at ambient temperature ($22 \pm 2^\circ$ C) until a clear saturated solution was obtained. The clear solution was removed by careful decantation, care being taken to avoid solid $Cd(OH)_2$ suspension.

2.4. *Scanning electron microscopy*

Sections (~ 5 mm thick) from the tips of the disposable working electrodes with attached cadmium deposits were gold-coated using a 'Polaron' sputter coater. Samples were examined in detail using a Cambridge Scientific Instruments S600 scanning electron microscope. Photographs were recorded on standard 35 mm film.

2.5. *Analytical*

The amount of cadmium deposited on the nickel rotating disc electrode was determined by dissolving the deposit in 1 mol dm^{-3} HCl and analysing using atomic adsorption spectroscopy (Varian Techtron AA5).

3. Results and discussion

3.1. *Stationary abraded nickel electrodes in 1.05×10^{-4} mol dm^{-3} $Cd(OH)_4^{2-}$/30% KOH*

During the course of this investigation a very large number of photographs were obtained of which only limited representative examples are presented here.

The morphology of cadmium deposits formed using 1.05×10^{-4} mol dm^{-3} $Cd(OH)_4^{2-}$ is potential dependent. At overpotentials η of -100 mV, 2D- fern-like dendrites were observed after prolonged deposition times of 66 h, an example is given in Fig. 1. There is a distinct regular branching of dendrites with little 'filling-in'. The dendrites are very thin and fragile and only loosely adherent to the electrode surface, great care being required

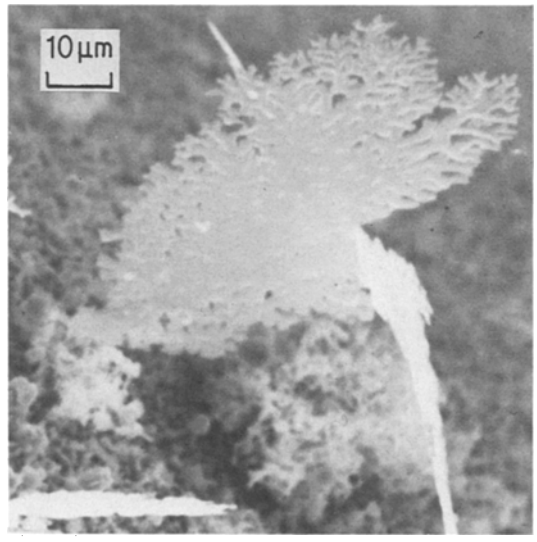

Fig. 1. Deposit morphology observed after 66 h deposition. 2D-Fern dendrite, $\eta = -100$ mV.

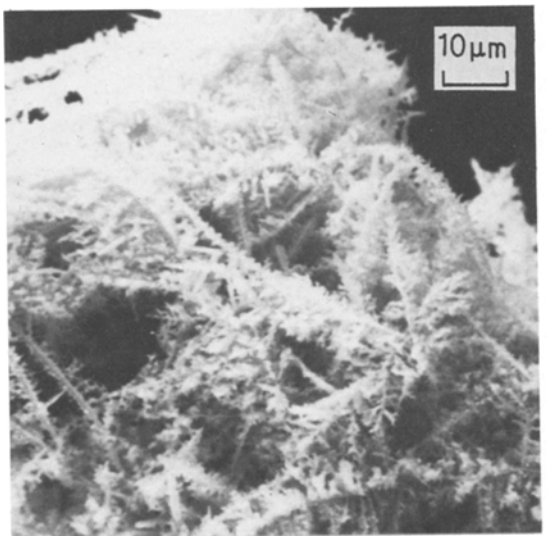

Fig. 2. Deposit morphology observed after 66 h deposition. Needle dendrite, $\eta = -200$ mV.

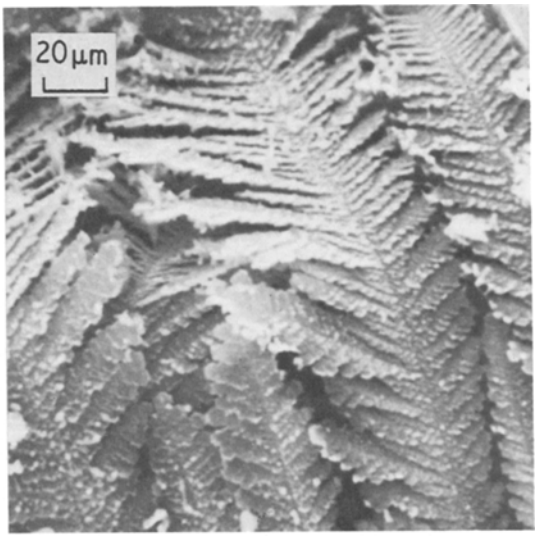

Fig. 3. Deposit morphology observed after 66 h deposition. Large fern dendrite, $\eta = -300$ mV.

during the removal of the electrode from the cell and preparation for SEM examination. Fig. 1 also illustrates the underlying electrode surface and gives some indication as to the probable state of the surface before dendrite growth started.

Fig. 2 shows examples of the needle-like dendrites formed at slightly higher overpotential (− 200 mV). These dendrites still retain some regular branching from the main stem but the secondary growths are relatively short. The needle-like dendrites grow to a greater length than the fern-like deposits previously described. For example, the ferns in Fig. 1 are typically 20 μm long whilst the needles in Fig. 2 are typically 30 μm long but in some instances they may be in excess of 100 μm. Table 1 summarizes the types and lengths of dendrites observed during potentiostatic deposition at stationary nickel wires.

On further increasing the overpotential to − 300 mV large fern-like dendrites result as shown in Fig. 3. The ferns here show more intergrowth (filling-in) than those observed at lower potentials. At higher magnification (Fig. 4) the constituent hexagonal cadmium platelets in a 'roof-tile' stacking formation are easily seen (cf. Wranglen [7]).

Similar morphologies to those shown in Figs. 1–3 were observed for galvanostatic deposition, small 2D-ferns below 30 $\mu A\,cm^{-2}$, needles and 2D-ferns from 20 to 50 $\mu A\,cm^{-2}$, and large filled in ferns from 50–75 $\mu A\,cm^{-2}$. The dendrite lengths are shown in Table 2.

3.2. *Stationary abraded nickel electrodes in 2.4×10^{-4} mol dm^{-3} $Cd(OH)_4^{2-}$/50% KOH*

The influence of concentration on the morphology

Table 1. Comparison of dendrite length and morphology obtained using stationary nickel substrates for two cadmate concentrations

66 h deposition 1.05×10^{-4} mol dm^{-3} $Cd(OH)_4^{2-}$/30% KOH			*24 h deposition* 2.4×10^{-4} mol dm^{-3} $Cd(OH)_4^{2-}$/50% KOH		
η (mV)	*Morphology*	*Average dendrite length* (μm)	η (mV)	*Morphology*	*Average dendrite length* (μm)
300	'in-filled' fern	40	200	needle	39
200	needle	31	100	fern	20
100	2D-fern	20	75	fine granular deposit	2

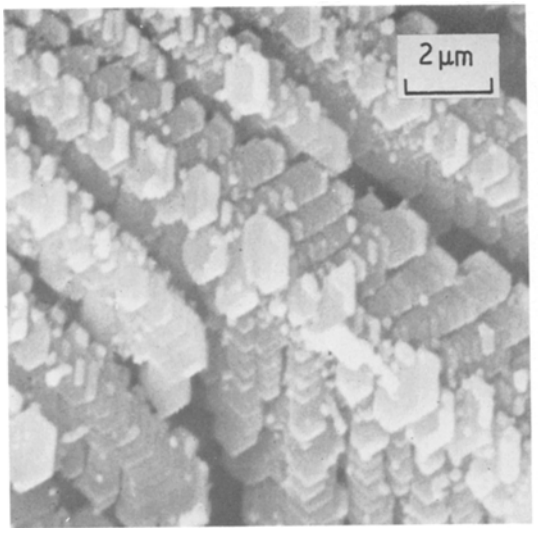

Fig. 4. Deposit morphology observed after 66 h deposition. Higher magnification of Fig. 3.

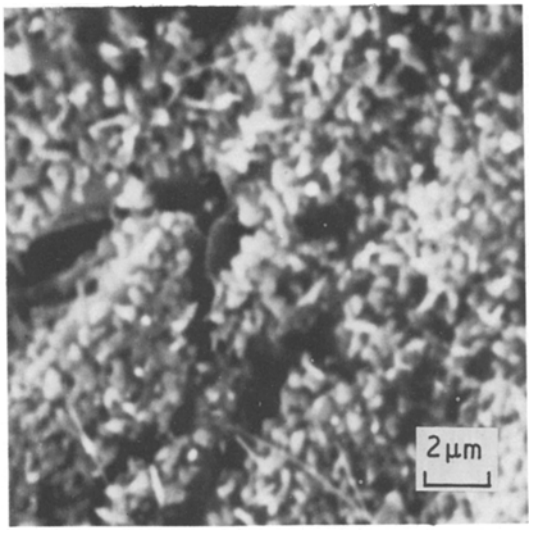

Fig. 5. Deposit morphology observed after deposition onto a nickel wire in 2.4×10^{-4} mol dm^{-3} $Cd(OH)_4^{2-}$/50% KOH. Fine deposit, $\eta = -75$ mV, 24 h deposition.

of cadmium deposits formed in alkaline media is difficult to study because of the low solubility of cadmate necessitating long deposition periods. Use of 50 wt % KOH allows an increase in $Cd(OH)_4^{2-}$ concentration by a factor of ~ 2.3 to be investigated. As anticipated it was found that the time to grow dendrites of a similar length at similar overpotentials was reduced in proportion to the increase in cadmate concentration (see Table 1).

The types of dendrite obtained at 2.4×10^{-4} mol dm^{-3} $Cd(OH)_4^{2-}$ were similar to those grown at the lower concentration and showed the same type of morphology dependence with overpotential. Fig. 5 illustrates the deposit formed at low overpotential (− 75 mV), whilst Figs. 6 and 7 illustrate the fern and needle-like dendrites formed at higher overpotentials (− 100 and − 200 mV, respectively), all after 24 h deposition time. If deposition is continued for longer periods a large mass of inter-twined dendrites results such as those in Fig. 8. The tips of these needle dendrites are well defined and as can be seen from Fig. 9 at higher magnification, show a sharp V-profile having an enclosed tip angle of $\sim 60°$.

It is possible that cadmium dendrites grow by the so-called twin plane re-entrant edge mechanism [13–15]. The main stem of the needle-dendrite is frequently observed to be made up of two sections with a distinct division between the halves

Table 2. Dendrite morphology and length for 24 h galvanostatic deposition of cadmium onto nickel wire in 1.05×10^{-4} mol dm^{-3} $Cd(OH)_4^{2-}$/30% KOH

Constant current (μA cm^{-2})	*Morphology*	*Dendrite length* (μm)	*Time* (h)
20	fern	11	24
30	needle	27.5	24
50	large filled-in fern	35	24

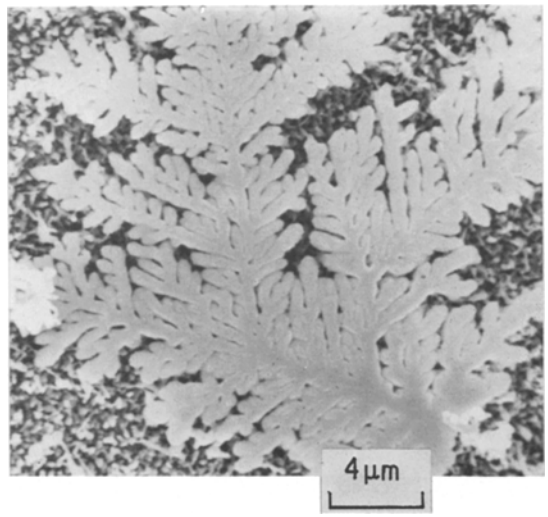

Fig. 6. Deposit morphology observed after deposition onto a nickel wire in 2.4×10^{-4} mol dm^{-3} $Cd(OH)_4^{2-}$/50% KOH. Fern dendrite, $\eta = -100$ mV, 24 h deposition.

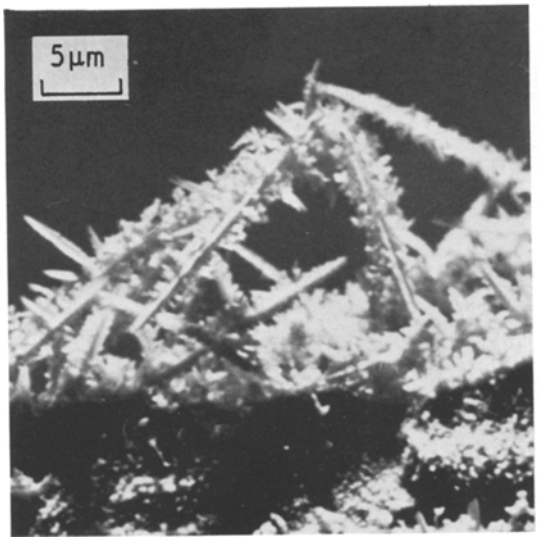

Fig. 7. Deposit morphology observed after deposition onto a nickel wire in 2.4×10^{-4} mol dm^{-3} $Cd(OH)_4^{2-}$/50% KOH. Needle dendrite, $\eta = -200$ mV, 24 h deposition.

(see for example Fig. 9). The main stem is often not co-planar and the 'back-bone' of the dendrite may be seen to be V-shaped (see for example Fig. 3).

However, a screw dislocation is also a particularly favourable site for dendrite initiation because it allows for continuous growth without the necessity for nucleation. Accordingly, dendrite

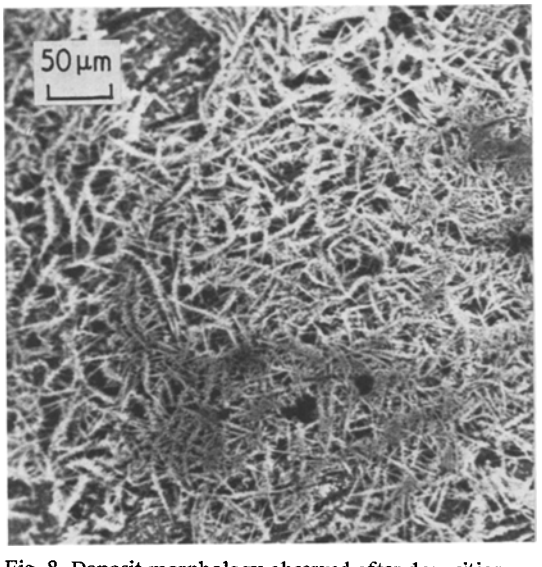

Fig. 8. Deposit morphology observed after deposition onto a nickel wire in 2.4×10^{-4} mol dm^{-3} $Cd(OH)_4^{2-}$/50% KOH. Inter-twinned dendrite, $\eta = -200$ mV, 124 h deposition.

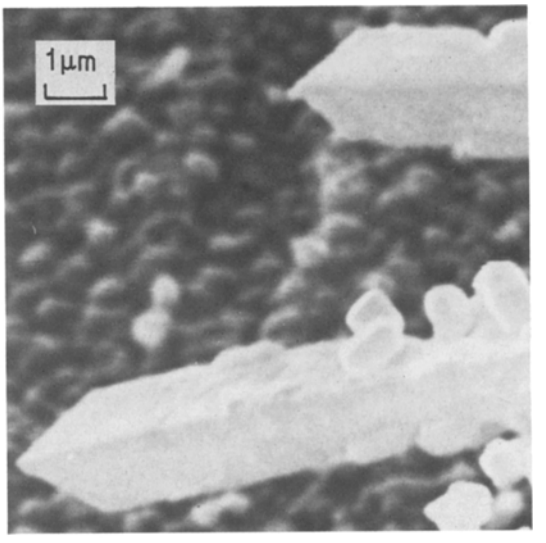

Fig. 9. Well defined dendrite tip.

growth via screw dislocations has been proposed [9] as an alternative to the twin plane re-entrant edge mechanism. Unfortunately, it is not possible to distinguish between the two mechanisms from this investigation. The presence of twinning could only be ascertained by other studies such as electron diffraction. Reddy [16] has suggested that the critical overpotential to initiate dendrite growth may be related to the stacking fault energy of the crystal lattice necessary for the formation of a twin plane used in dendrite propagation. The existence of twin planes in dendrites has been frequently reported, although it is not clear whether twin planes are in anyway essential to the dendrite growth process [17, 18].

The regularities in the side branches in terms of frequency and angle have been attributed to twinning phenomena [12]. Wranglen [7] has drawn attention to the importance of layered growth patterns during the growth of dendrites but these are manifestations of the later stages of growth and give little indication as to the dendrite origin.

3.3. *Polished rotating nickel disc electrodes in 1.05×10^{-4} mol dm^{-3} $Cd(OH)_4^{2-}$/30% KOH*

A particular advantage of using a rotating disc electrode (RDE) is that it allows the diffusional conditions at the electrode surface to be defined [19]. This facility is not possible with the abraded

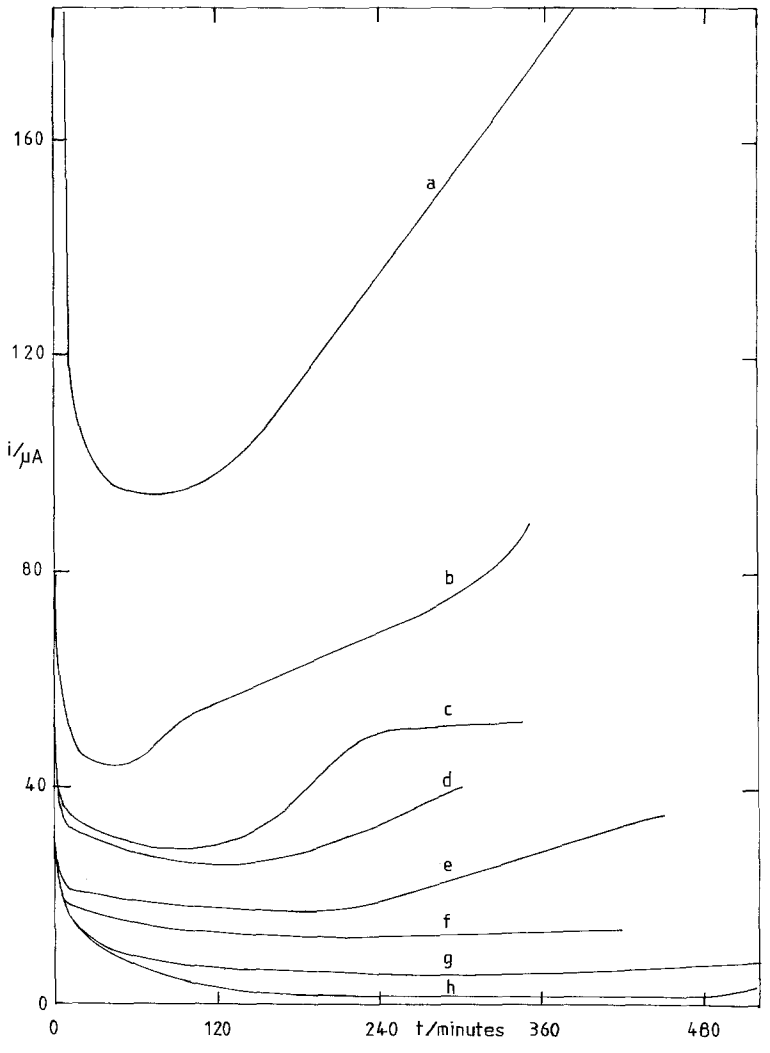

Fig. 10. Current against time curves for potentiostatic deposition of cadmium onto a rotating nickel disc electrode in 1.05×10^{-4} mol dm^{-3} $Cd(OH)_4^{2-}$/30% KOH for a range of overpotentials (a) — 375 mV, (b) — 350 mV, (c) — 325 mV, (d) — 300 mV, (e) — 275 mV, (f) — 250 mV, (g) — 180 mV, and (h) — 160 mV.

wires used in the earlier part of this study. At a rotation speed of 160.5 rad s^{-1} the diffusion layer thickness δ is 36 μm compared with ~ 100–200 μm for the stationary cases. Physical blockage of the electrode surface by hydrogen is also minimized by using an RDE because the gas bubbles are rapidly swept away.

Fig. 10 shows a family of current against time curves for potentiostatic deposition of cadmium onto an RDE over a range of overpotentials from — 160 to — 365 mV. In all cases the current falls rapidly during the first few minutes as a consequence of inhibition of the hydrogen reaction due to Cd-deposition. The measured current at any instant in time is made up of hydrogen evolution and cadmium deposition components with the hydrogen component dominating. At lower overpotentials (up to — 200 mV) a steady state condition is usually attained after about a 2 h period where the cadmium deposition and hydrogen evolution reactions compete for suitable sites on the electrode surface. In many cases, the coverage of the nickel surface by cadmium is incomplete and 'bare-patches' of exposed nickel can be found. At low overpotentials the current remains constant for several days showing little tendency to rise.

Fig. 11 shows the electrode surface after only 120 min deposition at an overpotential η of — 200 mV. Localized spots of cadmium can be seen on the nickel surface. At higher magnification (Fig. 12) this deposit displays a granular texture. Even after a longer deposition period, the type of deposit is not significantly altered. For example

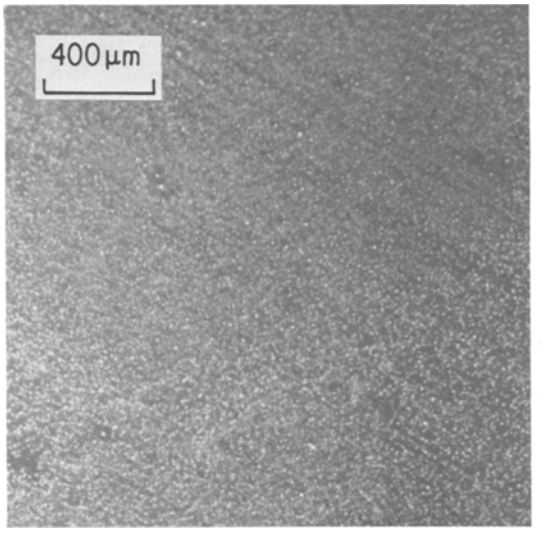

Fig. 11. Deposit morphology after deposition on a rotating nickel disc electrode in 1.05×10^{-4} mol dm^{-3} $Cd(OH)_4^{2-}$/30% KOH. Deposit after 120 min at $\eta = -200$ mV.

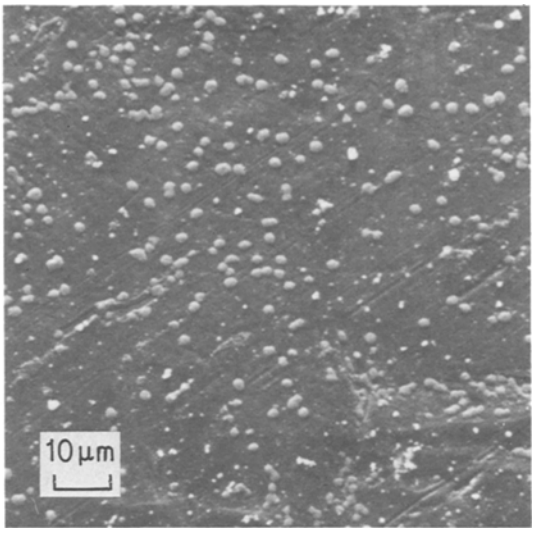

Fig. 13. Deposit morphology after deposition on a rotating nickel disc electrode in 1.05×10^{-4} mol dm^{-3} $Cd(OH)_4^{2-}$/30% KOH. Deposit after 21 h at $\eta = -165$ mV.

Figs. 13 and 14 show the type of deposit obtained after 21 h but at a lower overpotential ($\eta = -165$ mV). It should be noted that overpotentials of -165 mV are more than sufficient to reach limiting diffusion conditions at the electrode surface and indeed allowed dendrite growth to be observed using stationary wires after 24 h periods. Clearly additional criteria other than establishing a limiting diffusion current condition must be satisfied before dendrites appear.

At overpotentials above -250 mV, the current was found to increase after a latent period of between 1–3 h. This region of increasing current can be related to the appearance of a high surface area deposit or dendrites on the electrode surface. Fig. 15 shows the mass of cadmium determined

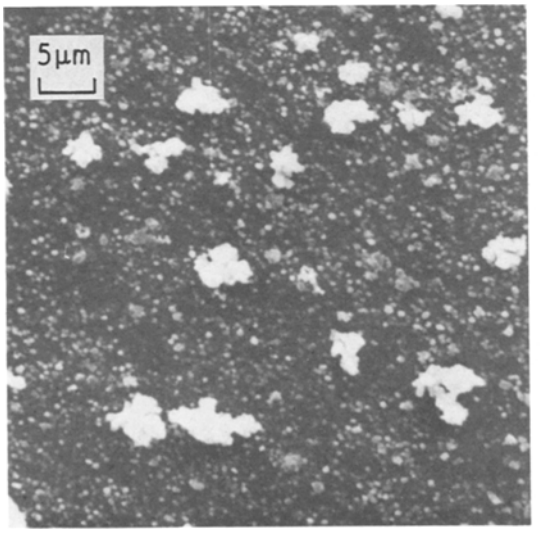

Fig. 12. Deposit morphology after deposition on a rotating nickel disc electrode in 1.05×10^{-4} mol dm^{-3} $Cd(OH)_4^{2-}$/30% KOH. Higher magnification of Fig. 11.

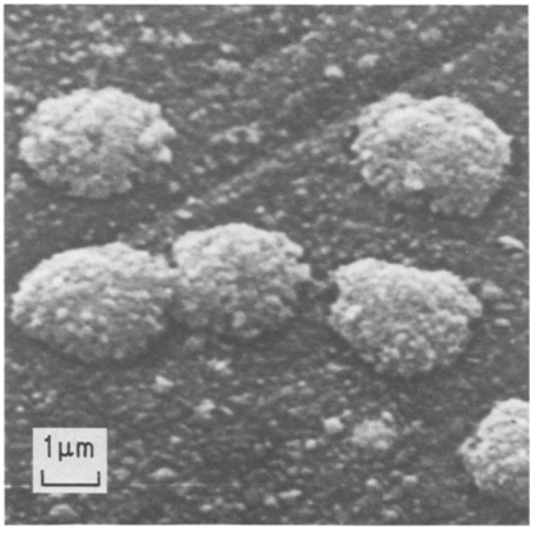

Fig. 14. Deposit morphology after deposition on a rotating nickel disc electrode in 1.05×10^{-4} mol dm^{-3} $Cd(OH)_4^{2-}$/30% KOH. Higher magnification of Fig. 13.

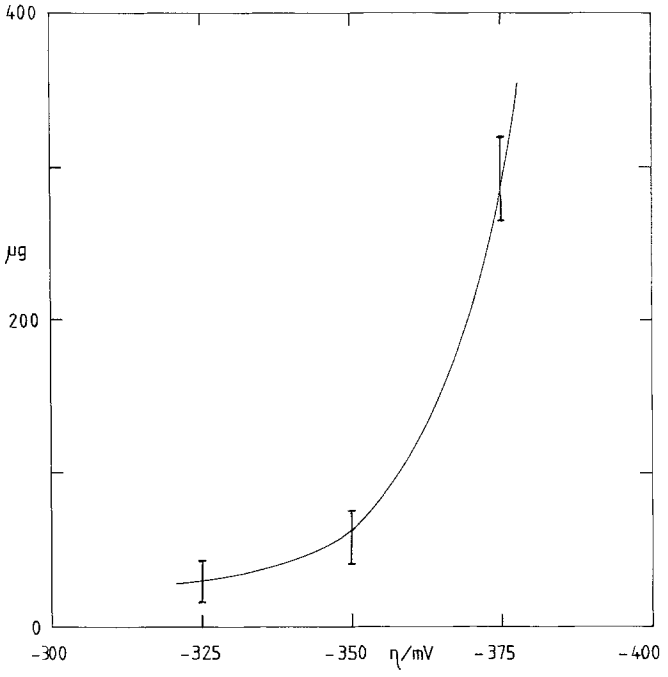

Fig. 15. Mass of cadmium deposited on a rotating nickel disc electrode in 1.05×10^{-4} mol dm^{-3} $Cd(OH)_4^{2-}$/30% KOH after 345 min at various overpotentials.

analytically on the RDE surface after deposition for 345 min at overpotentials between − 325 and − 375 mV. It is clear that the quantity of cadmium increases sharply over a relatively small range of overpotential and is consistent with current time curves of Fig. 10 at these values of overpotential. From the mass of cadmium deposited (~ 1.5 mg cm^{-2} after 345 min) at $\eta = -375$ mV it may be inferred from Faraday's Law that the average cadmium deposition current density is $\sim 20\,\mu$A cm^{-2}. Using the Levich equation [19] namely,

$$i_l = 0.62nFAD^{2/3}\nu^{-1/6}\omega^{-1/2}C \qquad (1)$$

where n = number of electrodes transferred, 2; F = Faraday's constant, 96 487 C mol^{-1}; A = electrode area, 0.196 cm^2; D = diffusion coefficient of $Cd(OH)_4^{2-} = 5.3 \times 10^{-6}$ cm^2 s^{-1}; ν = viscosity of 30% KOH, 0.0174 Stokes; ω = angular velocity, 160.5 rad s^{-1}; C = cadmate concentration, 1.05×10^{-7} mol cm^{-3}; a limiting current density of 18.6 μA cm^{-2}, in reasonable agreement with the analytical value is obtained.

Examination of the electrode surface after 120 min deposition at − 325 mV revealed similar overall features to those shown in Figs. 11–14. However, electrodes examined immediately after the increase in current (after 240 min) at the same overpotential revealed a considerable quantity of deposit on the electrode. A localized loose porous deposit was obtained after 240 min as in Fig. 16 which became still thicker (in spite of the relatively little further increase in current) after 330 min as in Fig. 17. After 390 min, a thick porous deposit spread across the electrode surface (as in Fig. 18) which under higher magnification

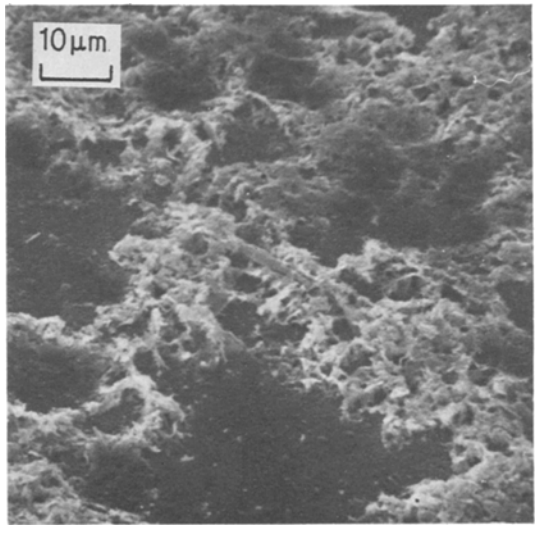

Fig. 16. Deposit morphology after 240 min deposition at $\eta = -325$ mV on a rotating nickel disc electrode in 1.05×10^{-4} mol dm^{-3} $Cd(OH)_4^{2-}$/30% KOH.

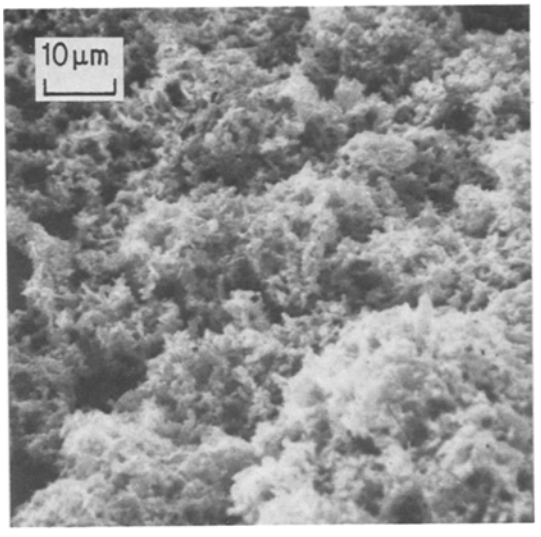

Fig. 17. Deposit morphology after 330 min deposition at $\eta = -325$ mV on a rotating nickel disc electrode in 1.05×10^{-4} mol dm^{-3} $Cd(OH)_4^{2-}$/30% KOH.

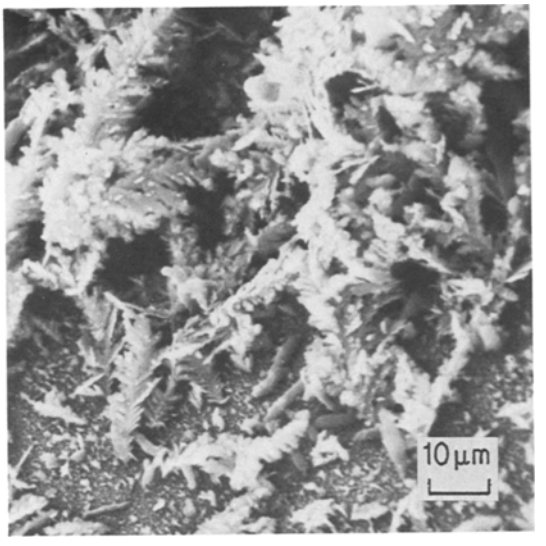

Fig. 19. Deposit morphology after 390 min deposition at $\eta = -325$ mV on a rotating nickel disc electrode in 1.05×10^{-4} mol dm^{-3} $Cd(OH)_4^{2-}$/30% KOH. Higher magnification of Fig. 18 showing fern dendrites.

(Fig. 19) was seen to be made up of small fern-like dendrites (up to 60 μm in length).

In general, whenever a significant increase in current was detected after the initial latent period, the deposit was found to consist of small fern-like dendrites of the type in Fig. 19. As expected, the dendrites tended to be longer when grown at higher overpotentials or for longer periods of time (see Table 3). The long needle-like growths found on the stationary wires under rather ill defined convective conditions were not observed on the rotating electrode. The slower development of dendrites on the rotating disc electrode even at relatively high potentials is probably related to the thinner diffusion layer pertaining to the rotating system compared to the stationary case. A thin diffusion layer would tend to restrict dendrite growth because the cadmate concentration profile would follow the surface macro-profile more closely and minimize initial amplification of surface roughness.

An additional factor which may have contributed to the extensive growth of dendrites on the stationary rough nickel wires might have been the presence of suspended $Cd(OH)_2$ trapped in the crevices during the growth process. Whilst reasonable precautions were taken to avoid gross amounts of suspended $Cd(OH)_2$ it was difficult to avoid

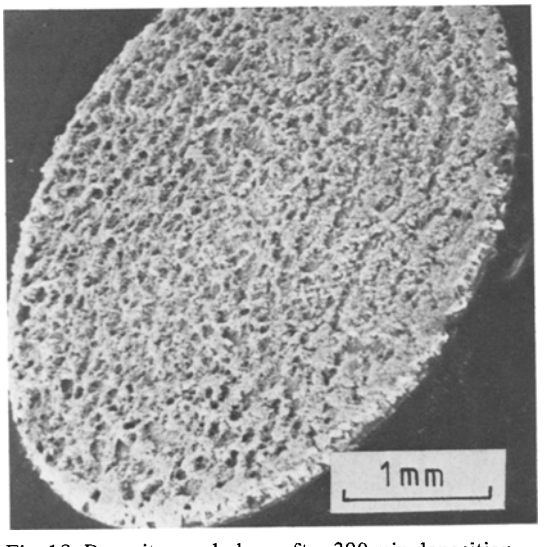

Fig. 18. Deposit morphology after 390 min deposition at $\eta = -325$ mV on a rotating nickel disc electrode in 1.05×10^{-4} mol dm^{-3} $Cd(OH)_4^{2-}$/30% KOH.

Table 3. Dendrite length with deposition time on a rotating nickel disc electrode at $\eta = -325$ mV *in* 1.05×10^{-4} mol dm^{-3} $Cd(OH)_4^{2-}$/30% KOH

Total deposition time (h)	*Average dendrite length* (μm)
4	22
$5\frac{1}{2}$	43
$6\frac{1}{2}$	66

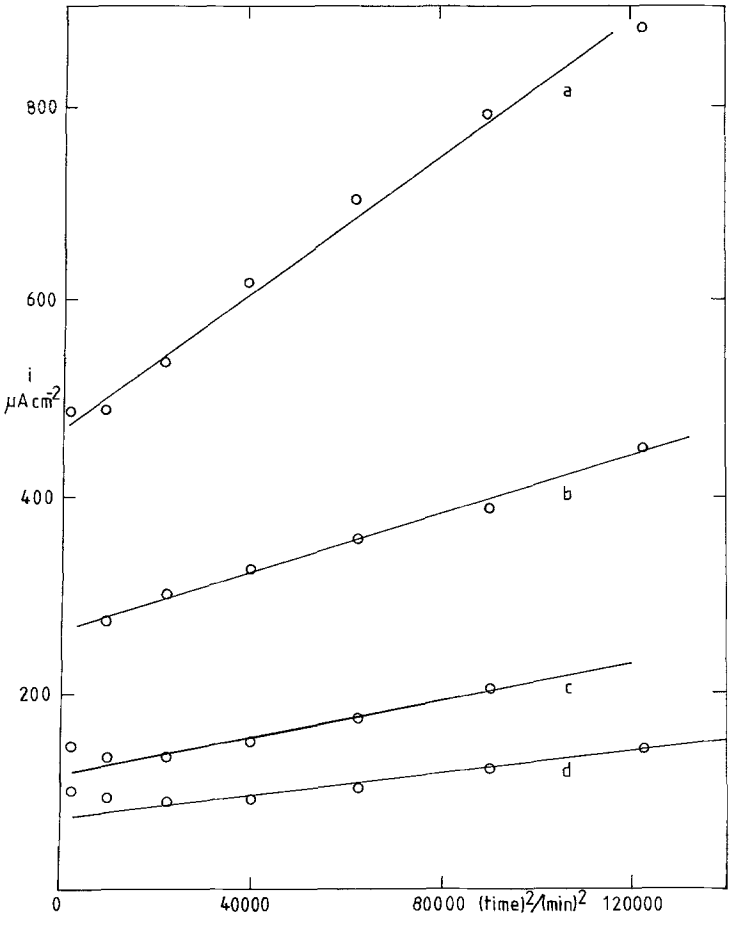

Fig. 20. Current density against (time)^2 for data taken from Fig. 10 for a range of overpoentials (a) — 375 mV, (b) — 350 mV, (c) — 300 mV, and (d) — 275 mV.

small quantities of colloidal material or $Cd(OH)_2$ crystallizing from the solution in the longer term experiments (66 h).

A concurrent study at the University of Newcastle [20] has drawn attention to the influence of $Cd(OH)_2$ suspension on the rate of dendrite growth. Extremely small amounts of $Cd(OH)_2$ suspension may lead to a disproportionate growth in the dendrites.

The minima in the current–time curves of Fig. 10 give an approximate measure on the induction time t_i before dendrite growth takes place. The upturn in current is related to the avalanche growth region when the electrode surface area is rapidly increasing. It can, therefore, be used as a guide to indicate the likely presence of dendrites. However, it is only reliable when the ratio of the area due to dendrites relative to the planar surface is significant. Thus, a few small dendrites could be present on an electrode surface without any significant increase in current being registered. According to Diggle *et al.* [9] in the avalanche growth region the dendrite current, i, is proportional to the square of the time, t, indicative of progressive rather than instantaneous initiation and growth.

Fig. 20 shows a plot of i against t^2 for the data taken from Fig. 10 for a range of overpotentials η from — 275 to — 375 mV. It can be seen over a significant time scale that i is indeed proportional to t^2, the slope of the plots increasing with applied overpotential as expected. From the data of Fig. 20 it is possible to estimate the rate of dendrite growth, however, detailed discussion will be deferred to the third part of this investigation.

3.4. *Stationary polished cadmium electrodes in* 1.05×10^{-4} *mol dm*$^{-3}$ $Cd(OH)_4^{2-}$*/30% KOH*

The deposition of cadmium onto a polished cadmium substrate was investigated to establish whether the long induction period was associated

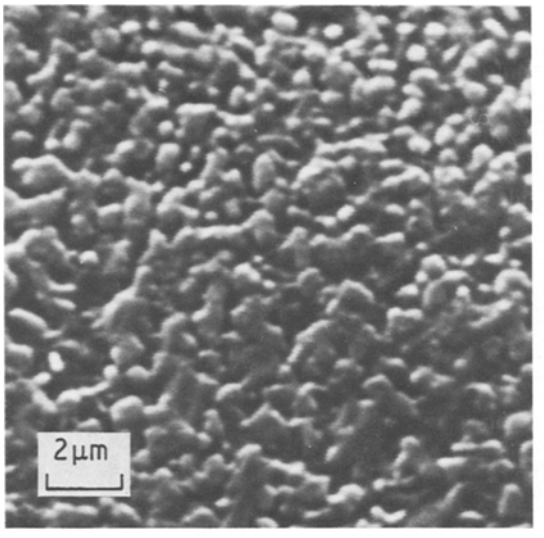

Fig. 21. Deposit morphology after deposition on a cadmium wire in 1.05×10^{-4} mol dm^{-3} $Cd(OH)_4^{2-}$/30% KOH. 3 h at $\eta = -200$ mV.

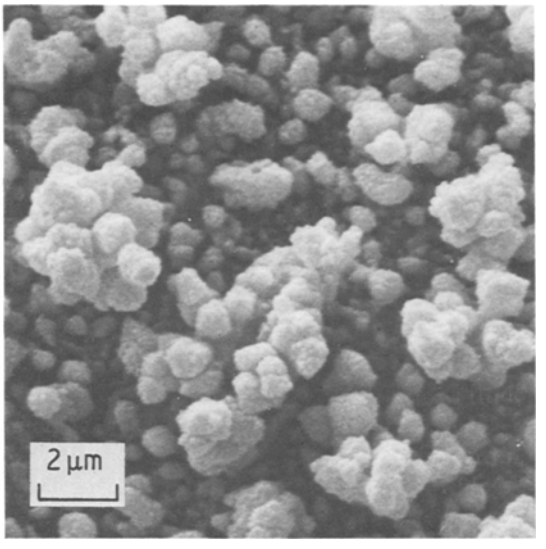

Fig. 22. Deposit morphology after deposition on a cadmium wire in 1.05×10^{-4} mol dm^{-3} $Cd(OH)_4^{2-}$/30% KOH. 24 h at $\eta = -200$ mV, nodular dendrite precursors.

with the nature of the substrate. Because nickel and cadmium have different crystal structures (f c c and h c p, respectively), some intermediate structure might be necessary before cadmium dendrites can propagate. There is also the possibility of the formation of nickel cadmium alloys, e.g. Ni_5Cd_{21} [4] in the surface region and also interdiffusion of cadmium into the base substrate when nickel is used. Such effects are eliminated when a cadmium substrate is used. Nevertheless, the nickel substrate is more relevant to the nickel cadmium battery system, because of the use of nickel as an electrode support material.

Fig. 21 shows the surface of a cadmium electrode after 3 h deposition at an overpotential η of -200 mV. At this stage only a grainy deposit with some crystallographic alignment is present, but dendrites are absent. It should be noted that as in the case of the nickel substrate hydrogen evolution is also taking place as well as cadmium deposition at $\eta = -200$ mV. When the deposition time is increased to 24 h as in Fig. 22, nodular dendrite precursors can readily be identified, as well as dendrites of length up to 60 μm composed of nodular aggregates as in Fig. 23.

If the growth process is studied at higher overpotential ($\eta = -300$ mV) then both the dendrite precursors and final dendrites become distinctly more crystalline in character. Fig. 24 shows the deposit obtained after 7 h deposition at $\eta = -300$ mV. Small ($< 4\,\mu$m) elongated cadmium crystallites displaying sharp tips with enclosed angles of $\sim 60^\circ$ can be clearly identified. It seems highly likely that the tip-shape found for the fully developed dendrite is determined at this stage of growth, the tip shape remaining largely unchanged as the dendrites increase in length. Once the tip radius has been reduced sufficiently (in the range

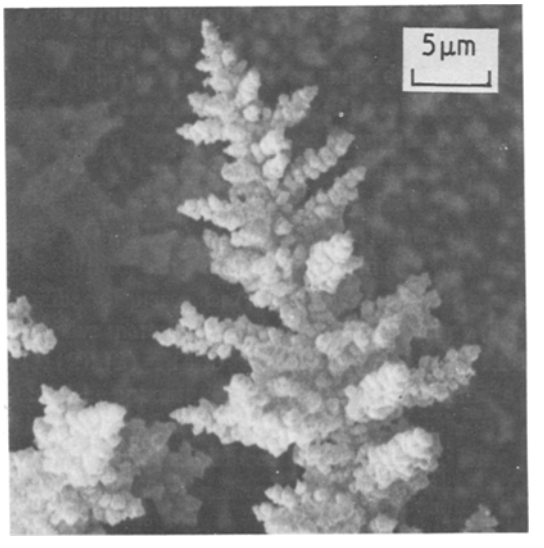

Fig. 23. Deposit morphology after deposition on a cadmium wire in 1.05×10^{-4} mol dm^{-3} $Cd(OH)_4^{2-}$/30% KOH. 24 h at $\eta = -200$ mV, dendrites.

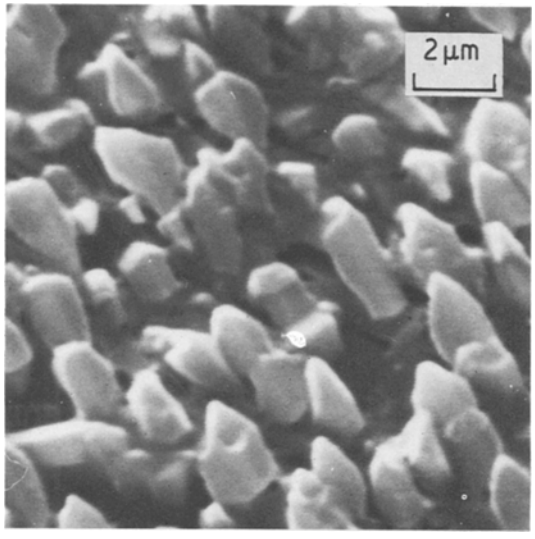

Fig. 24. Deposit morphology after deposition on a cadmium wire in 1.05×10^{-4} mol dm^{-3} $Cd(OH)_4^{2-}$/30% KOH. 7 h at $\eta = -300$ mV.

0.01 to 0.1 μm) spherical diffusion can commence at the tip. Provided that a distinct concentration difference can be distinguished at the tip compared with the planar surface (i.e. the critical height has been attained) rapid dendrite growth ensues.

Fig. 25 shows examples of the needle-like dendrites after 18 h deposition at − 300 mV. The dendrite lengths were typically found to be of the order of 50 μm.

From the results obtained, it appears that the long induction period (~ 8 h) is associated primarily with the low concentration (1.05×10^{-4} mol dm^{-3}) of depositing metal complex ion, $Cd(OH)_4^{2-}$ rather than to the nature of the substrate. An induction period of several hours appears to be necessary at low concentration irrespective of whether a polished nickel or cadmium substrate is used.

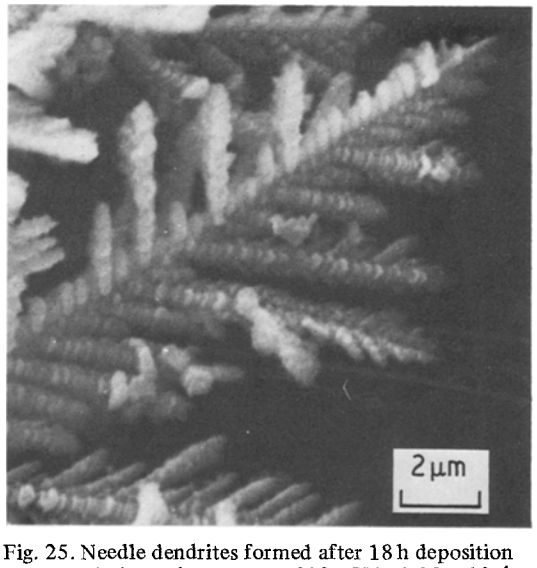

Fig. 25. Needle dendrites formed after 18 h deposition onto a cadmium wire at $\eta = -300$ mV in 1.05×10^{-4} mol dm^{-3} $Cd(OH)_4^{2-}$/30% KOH.

4. Conclusion

Studies using stationary nickel wire substrates at low overpotentials ($\eta = -100$ mV) have shown that 2D-fern like dendrites (~ 20 μm long) can be obtained after long deposition periods (66 h) in 30% KOH containing 1.05×10^{-4} mol dm^{-3} $Cd(OH)_4^{2-}$. At intermediate potentials (η, − 200 mV) needle-like dendrites, of length in excess of 100 μm result. Higher overpotentials (η, − 300 mV) appear to lead to reversion to a fern-like morphology showing considerable intergrowth. The fern-like dendrites reveal a characteristic stacking of hexagonal cadmium platelets in a roof-tile formation. The needle dendrites had V-shaped tip profiles with enclosed angles of 60°, and the shorter side-arms also appear to be inclined to the stem at the same angle. This feature would be expected for a metal like cadmium having a hexagonal close-packed lattice. No conclusive evidence can be offered from this work to distinguish between the twin plane re-entrant groove mechanism and rotation of screw dislocations as the mechanism for dendrite growth.

Similar results were obtained using 50% KOH containing 2.4×10^{-4} mol dm^{-3} $Cd(OH)_4^{2-}$ except that the time taken to grow dendrites of an equivalent length and morphology was proportionally reduced.

Potentiostatic current, i, against time, t, curves for cadmium deposition onto a Ni-RDE show initially a rapid fall in current due to blockage of hydrogen evolution sites by cadmium. At low overpotentials (< − 200 mV) the current remained at a low and constant value for several hours (days). At higher overpotentials (> − 200 mV) the current passed through a distinct minimum after an induction time t_i (1–3 h). SEM examination of the electrode surface revealed that the rise in current coincided with the presence of fern-like dendrites (20–60 μm long). At lower overpoten-

tials (< -200 mV) after 24 h deposition only a granular non-dendritic deposit was observed. Long needle like dendrites were not observed using the RDE system. Plots of i against t^2 were found to be linear suggesting progressive rather than instantaneous initiation of dendrite growth.

Dendrites grown onto a polished stationary cadmium substrate resembled those on the nickel wire. An appreciable induction time (~ 8 h) was also required indicating that the substrate type alone was not responsible for the long induction period. The long induction period and slow rate of dendrite growth appears to be primarily associated with the low concentration of soluble cadmium species in alkaline solution.

Acknowledgements

The authors thank the Directors of the Berec Group Limited for permission to publish this work. The authors are also indebted to Dr R. D. Armstrong and Mr S. Churchouse of the University of Newcastle for many helpful discussions. Thanks are also due to Mr D. J. Buckle for assistance with scanning electron microscopy.

References

[1] P. Bauer, 'Batteries for Space Power Systems', NASA Report SP-172.

[2] K. L. Dick, T. Dickinson, R. J. Doran, S. A. E. Pomroy and J. Thompson, 'Power Sources 7' (Proceedings of the 11th International Power Sources Symposium) (edited by J. Thompson), Academic Press, London (1979) p. 195.

[3] K. L. Dick, PhD thesis, Newcastle University (1978).

[4] R. Barnard, *J. Appl. Electrochem.* **11** (1981) 217.

[5] P. B. Price, *Phil. Mag.* **4** (1959) 1229.

[6] G. Poli and L. Peraldo Bicelli, *L. Metall. Italiana* **54** (1962) 497.

[7] G. Wranglen, *Electrochim. Acta* **2** (1960) 130.

[8] J. L. Barton and J. O'M. Bockris, *Proc. Roy. Soc.* **A268** (1962) 485.

[9] J. W. Diggle, A. R. Despic and J. O'M. Bockris, *J. Electrochem. Soc.* **116** (1969) 1503.

[10] K. I. Popov, M. D. Maksimovic and J. D. Trnjancev, *ibid.* **11** (1981) 239.

[11] A. R. Despic and M. M. Purenovic, *ibid.* **121** (1974) 329.

[12] A. R. Despic and K. I. Popov in 'Modern Aspects of Electrochemistry, No. 7', (edited by B. E Conway and J. O'M. Bockris), Plenum Press, New York (1972) Ch. 4.

[13] J. B. Kushner, *Metal. Prog.* **81** (1962) 88.

[14] H. Fisher, 'Elektrolytishe Abscheidung und Elektrokristallisation von Metallen', Springer Verlag, Berlin (1954).

[15] M. T. George and V. K. Vaidyan, *J. Appl. Electrochem.* **12** (1982) 359.

[16] T. B. Reddy, *J. Electrochem. Soc.* **113** (1966) 117.

[17] N. A. Pangarov, *Phys. Status Solidi* **20** (1967) 371.

[18] N. A. Pangarov, *Electrochim. Acta* **13** (1968) 1641

[19] V. G. Levich, 'Physicochemical Hydrodynamics', Prentice-Hall, Englewood Cliffs, New Jersey (1962).

[20] R. D. Armstrong and S. Churchouse, private communication.